Supporting Information

Characterization of Porous Materials by Fluorescence Correlation Spectroscopy Super-resolution Optical Fluctuation Imaging

*Lydia Kisley,[1] Rachel Brunetti,[2] Lawrence J. Tauzin,[1] Bo Shuang,[1] Xiyu Yi,[3] Alec W. Kirkeminde,[4] Daniel A. Higgins,[4] Shimon Weiss,[3,5,6] * Christy F. Landes,[1,7] **

[1] Department of Chemistry, Rice University, Houston, TX 77251

[2] Department of Physics, Scripps College, Claremont, CA 91711

[3] Department of Chemistry and Biochemistry, University of California Los Angeles, Los Angeles, CA 90095

[4] Department of Chemistry, Kansas State University, 213 CBC Building, Manhattan, Kansas 66506-0401, United States

[5] Department of Physiology, University of California Los Angeles, Los Angeles, CA 90095

[6] California NanoSystems Institute, University of California Los Angeles, Los Angeles, CA 90095

[7] Department of Electrical and Computer Engineering, Rice University, Houston, TX 77251

AUTHOR INFORMATION

Corresponding Author

*Phone: 713-348-4232. E-mail: cflandes@rice.edu and sweiss@chem.ucla.edu.

TABLE OF CONTENTS

Information on methods and analysis:

fcsSOFI resolution improvement at pore boundaries

The importance of fcsSOFI is to map porous structures. fcsSOFI provides further improvement in resolution to resolve the adjacent boundaries of multiple pores. Assuming emitters cannot diffuse among different pores (or lose all memory of previous diffusion once entering another pore), cross-correlation between different pores are zero, giving:

$$(S1)\ \ G_2(r,\tau) = \sum_{pore_i} \int_{r_1, r_2\ in\ pore_i} dr_1 dr_2 U(r-r_1)U(r-r_2) \frac{\langle C \rangle}{(4\pi D\tau)^{1.5}} \exp\left(-\frac{(r_1-r_2)^2}{4D\tau}\right) \varepsilon_1 \varepsilon_2$$

This change makes the contribution of cross-correlation terms smaller compared to the auto-correlation terms. In the limiting case, where every single position is an isolated pore, we simply have $r_1 = r_2$ and $G_2(r,\tau) \sim \int dr_1 U(r-r_1)^2 \varepsilon_1 \varepsilon_2$ reduces to the standard 2nd order SOFI situation for fluctuating emitters.

Range of emitter concentration and diffusion coefficients for fcsSOFI performance and comparison to SPT

fcsSOFI analysis relies on intensity fluctuation in each pixel to reconstruct the higher resolution image and extract diffusion coefficients at different regions. Therefore, fcsSOFI has very similar requirements on emitter concentration and measurable diffusion coefficient ranges to traditional FCS. For a concentration range of 10^{-9} ~ 10^{-6} M the average number of molecules in a femtoliter FCS focal volume is 0.1 ~ 1000.[1] For our detector, the corresponding number of emitters per pixel should be 0.001~10. The resolvable diffusion coefficients depend on the frame duration and number of frames in the sequence:

$$(S2)\ \ \frac{2\sigma_{xy}^2}{4T} < D < \frac{2\sigma_{xy}^2}{4dt}$$

where dt is the time lag between frames, and T is the total time of the sequence used for correlation analysis. In this work, dt is 0.04s and T is 40s (see Methods) and a reasonable range for observable diffusion coefficients was calculated to be 10^2~10^6 nm^2/s based on Equation 6 (Figure S1).

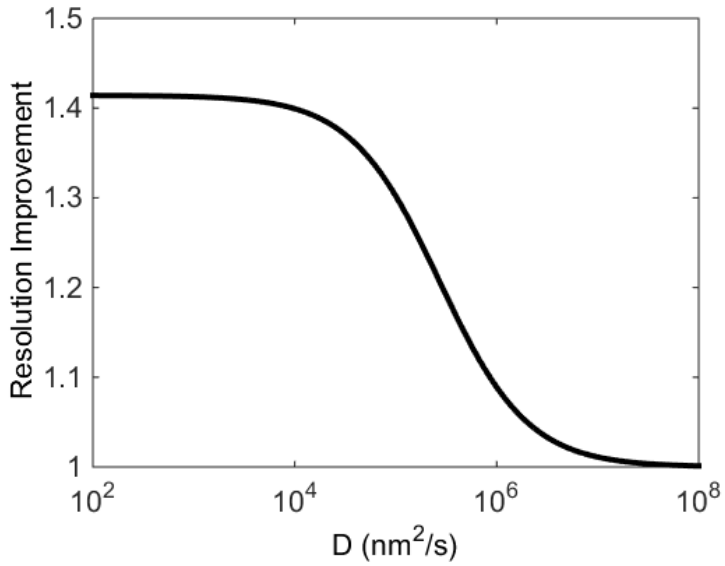

Figure S1. fcsSOFI resolution improvement over a range of diffusion coefficients. D = 10^2 - 10^8 nm^2/s and the resolution improvement is calculated by Equation 6. The resolution improvement represents the improvement based on 2nd order correlation alone, without deconvolution.

In comparison to SPT, the corresponding density of emitters should be much lower, ~ <0.01 emitters per pixel, based on a PSF size that expands over ~ 3 x 3 pixels (or ~ 10 $pixels^2$), compared to the range for fcsSOFI (0.001~10 emitters/pixel). The range of diffusion coefficients 10^2~10^6 nm^2/s corresponds to 3 nm - 350 nm (< 6 pixels) displacement between individual frames, which corresponds to a reasonable range for SPT methods to be successful with emitters with high signal and low density of emitters. SPT should obtain diffusion information from shorter data series, requiring 10-100's of frames, under those carefully designed experimental

conditions compared to fcsSOFI which calculates averaged information over ~100-1000's of frames.

Selection of emitters for fcsSOFI

fcsSOFI can work with a variety of emitters, diverse in radiative mechanism and size. In the current experimental work two types of emitters were utilized that produce light by fluorescence: 100 nm orange fluorescent polystyrene beads and single molecule DTPDI fluorophores. fcsSOFI analysis would be compatible with materials that produce optical signals by other means as long as the signal fluctuates with time due to diffusion, similar to the reports of SOFI with non-fluorescent probes.[2] Scattering from nanoparticles, photon luminescence in plasmonic nanomaterials, Raman scattering, and semiconductor quantum dots are all possible optical probes that could be used in fcsSOFI. Further, fcsSOFI should theoretically work with complex systems with multiple emitters that vary in size or color. Considerations of the species-dependent brightness and diffusion constants should be strategically selected so the convolved signal in the resulting autocorrelation signal can be resolved. The result would be two fcsSOFI maps with the same spatial saturation value but different hues representing the independent diffusion properties of different sized probes. Mixtures of spectrally separated emitters for microscopes capable of multi-channel detection could also be used. For further discussion, readers should refer to studies of complex mixtures that have been performed by FCS.[3, 4] Future work will pursue the possibilities of emitter optical signal mechanisms, size, and mixtures.

Supplementary work on super-resolution capabilities of fcsSOFI analysis by simulation:

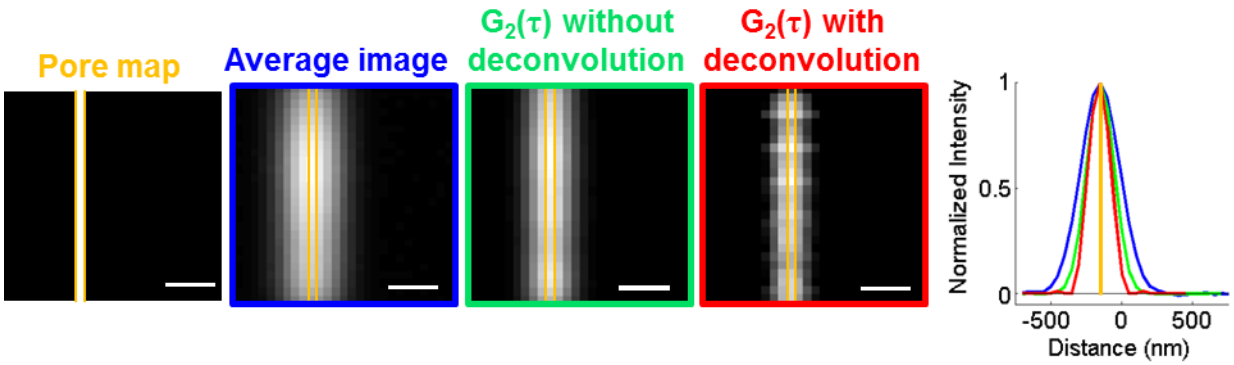

Figure S2. Single pore simulation quantifies resolution enhancement.
A simulation of a single emitter in a single one-dimensional pore undergoing Brownian diffusion with D = 1 x 10^5 nm^2/s was performed to quantify the resolution enhancement. The (blue) average image, (green) second-order autocorrelation data before performing deconvolution, (red) second-order autocorrelation data after performing deconvolution are shown with the respective (right) line section profiles averaged across all y showing the full width at half maximum (fwhm) of the pore for each analysis. The color in the line section corresponds to the border colors of the images. Orange lines in each image indicate the true pore location. Empirically, second-order autocorrelation alone improves the fwhm by a factor of 1.4 and with deconvolution improves by a factor of 1.9. All scale bars are 300 nm.

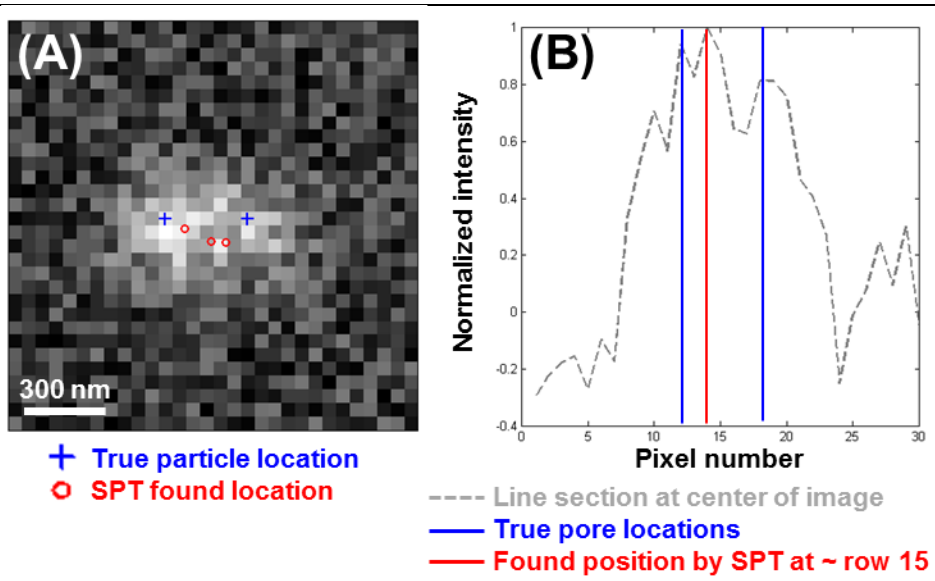

Figure S3. Mislocalization of true pore locations found by diffraction-limited imaging and single particle tracking.
The overlap of PSFs when particles are close to one another in the two separate pores cause the average intensity centroid to be shifted in the diffraction-limited image and mislocalization of the centroid positions for SPT results. In the example frame shown in (A), two emitters in neighboring pores are located at the same vertical location. The SPT localizations for the single frame are indicated in red, and are not at the true particle locations, indicated by blue. (B) The line section intensity trace taken across the center of the image shows the maximum peak is not at the true pore locations. This shows the overlapping of low signal PSFs can cause both average intensity and SPT to result in false shifts of the true pore locations, explaining the shift of the gray and orange peaks towards the center in Figure 1j. Overlapping PSFs would occur more often in samples with a high density of emitters, but Figure S3 shows that even at a low density of two emitters in our simulation, overlapping PSFs leading to false localizations still occur.

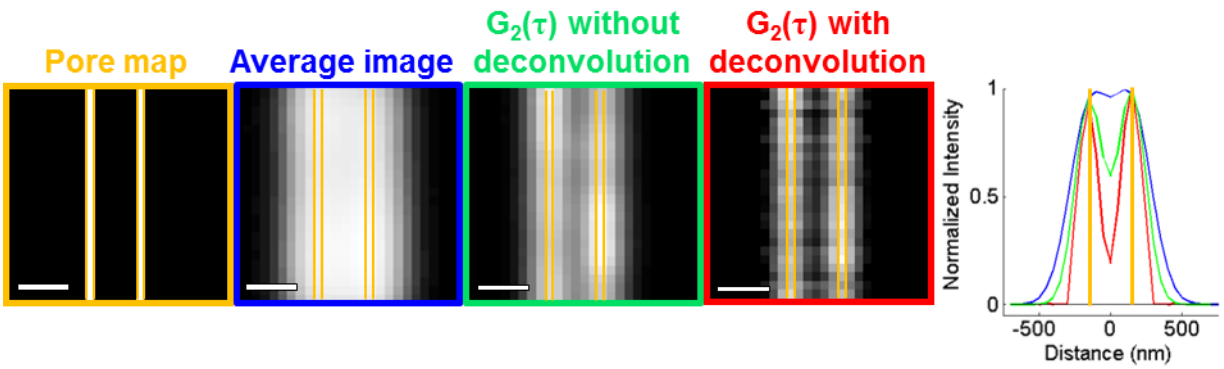

Figure S4. Comparison of resolution enhancement with and without deconvolution. Data reported in Figure 1g, i, and j with the addition of the (green) second-order autocorrelation data before performing deconvolution. (Right) Line sections averaged across all y from each image to compare relative fwhm. The color in the line section corresponds to the border colors of the images. Orange lines in each image indicate true pore location. Second-order autocorrelation alone resolves the two pores at a normalized intensity of 0.7 but not at the fwhm. All scale bars are 300 nm.

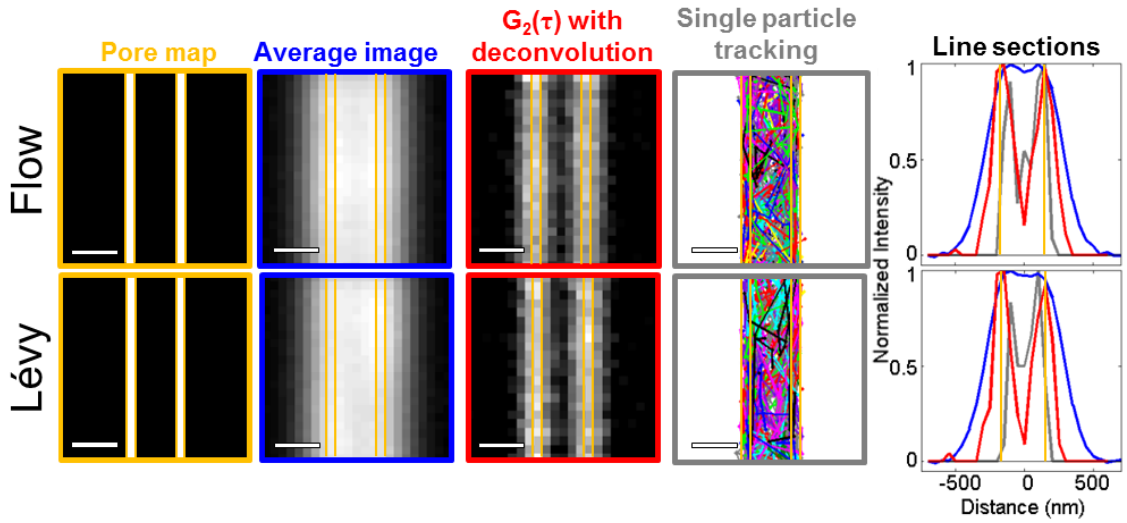

Figure S5. Super-resolution information can be achieved by fcsSOFI analysis of different types of diffusion.

The same pore map of two neighboring one-dimensional pores illustrated in Figure 1f was used. (top) Diffusion under flow was simulated by having an unequal probability of taking a step in the positive (p_{up}) or negative (p_{down}) direction (p_{up} = 0.7, p_{down} = 1 - p_{up} = 0.3). (bottom) Anomalous diffusion was simulated as a Lévy walk where the step size is taken from a power-law probability distribution with an exponent of $\alpha = 1.5$, as opposed to a normal distribution. As in Figure 1g-j, comparisons of the (blue) average, (red) SOFI, and (gray) SPT images were made. (Right) Line sections averaged across all y show similar improvements in the fwhm by factors of ~2 were observed for fcsSOFI. The color in the line section corresponds to the border colors of the images. Other simulations with flow probabilities of 0.9, 0.7, and 0.3, heterogeneity of flow probabilities being different in each pore, and Lévy exponents of $\alpha = 1.3$ and 1.7 were analyzed to verify the universality of the method. Similar results in resolution enhancement were observed. Orange lines in each image indicate true pore location. All scale bars are 300 nm.

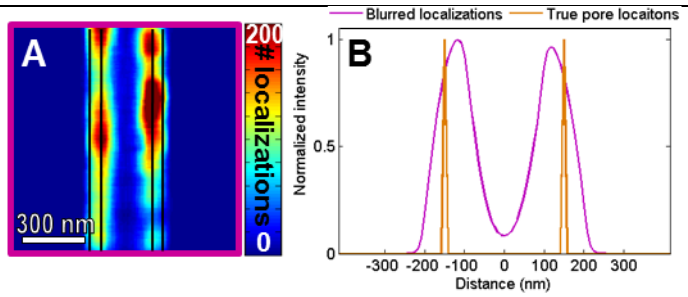

Figure S6. Representation of SPT data in Figure 1h by blurred PSF localization. Each centroid location found is represented by Gaussian with an amplitude of one and standard deviation of 81 nm, representing the localization accuracy of our SPT analysis. (A) Blurred representation super-resolution image. Black lines indicate true pore location. (B) Line section averaged across all y from blurred image to compare relative fwhm to true pore locations. Similar to Figure 1j, the center locations of the pores are misaligned compared to the true location due to the overlap of the PSFs.

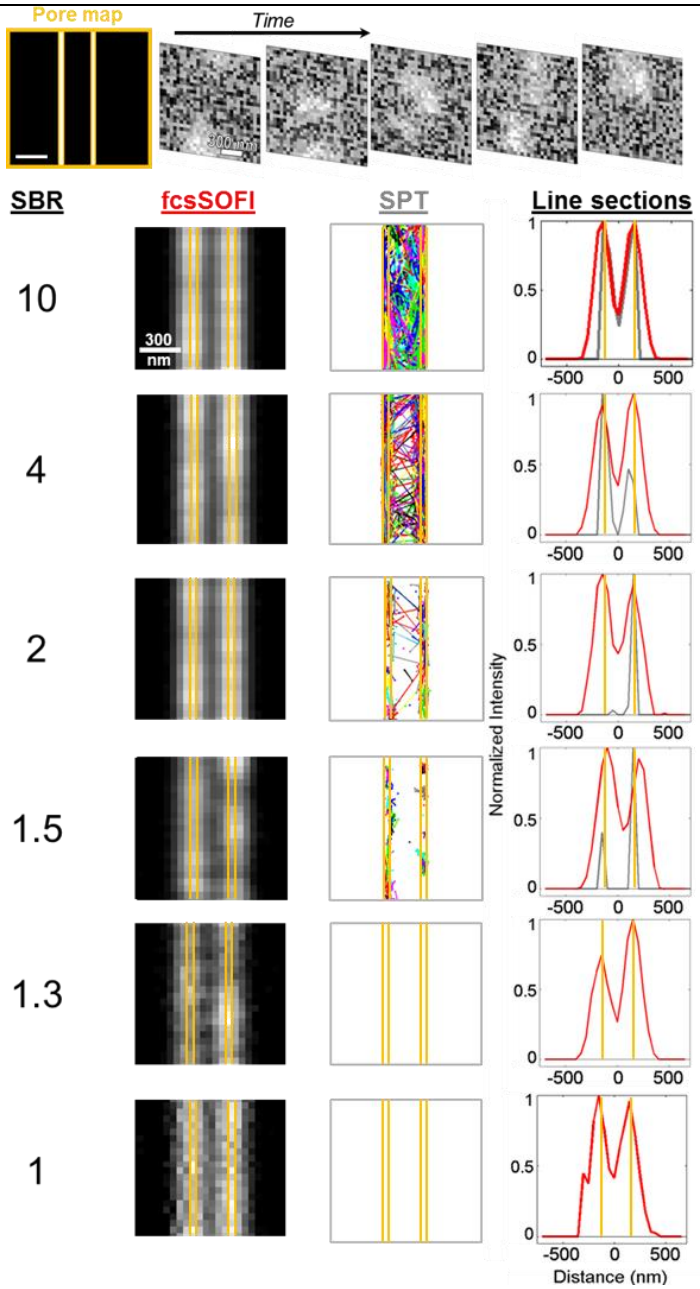

Figure S7. fcsSOFI analysis produces super-resolution data under low signal-to-background ratio conditions where localization-based single particle tracking fails. (Top) Example series of frames with four total emitters (two in each pore) undergoing 1D Brownian diffusion ($D_{left} = D_{right} = 1 \times 10^5$ nm^2/s) at a SBR of 1. (Bottom) Example (left) fcsSOFI results compared to (center) SPT localizations with (right) line sections taken across the center of the image for SBR ranging from 1-10. SPT localization under SBR ≤ 2 is challenging, resulting in no emitters being identified (SBR = 1, 1.3) or undersampling with mislocalization between the pores (SBR = 1.5, 2). Comparable results are observed for correlation at all SBRs where two pores are resolved at the fwhm. Orange lines in each image indicate true pore location. All scale bars are 300 nm.

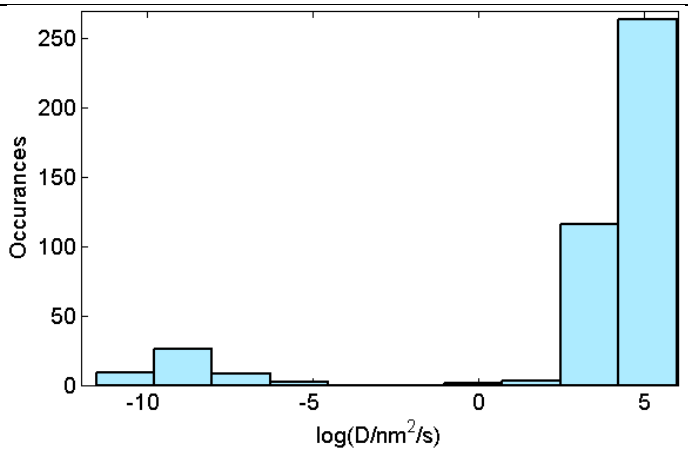

Figure S8. Distribution of diffusion coefficients from single particle tracking analyzed by maximum likelihood estimator analysis.[5]

Using the MATLAB curve fitting toolbox, the two populations from a two-term Gaussian fit are $\log(D_1/\mathrm{nm}^2\cdot\mathrm{s}^{-1}) = -8.9 \pm 1.7$ and $\log(D_2/\mathrm{nm}^2\cdot\mathrm{s}^{-1}) = 4.7 \pm 1.5$ with relative contributions of $8 \pm 1\%$ and $92 \pm 8\%$.

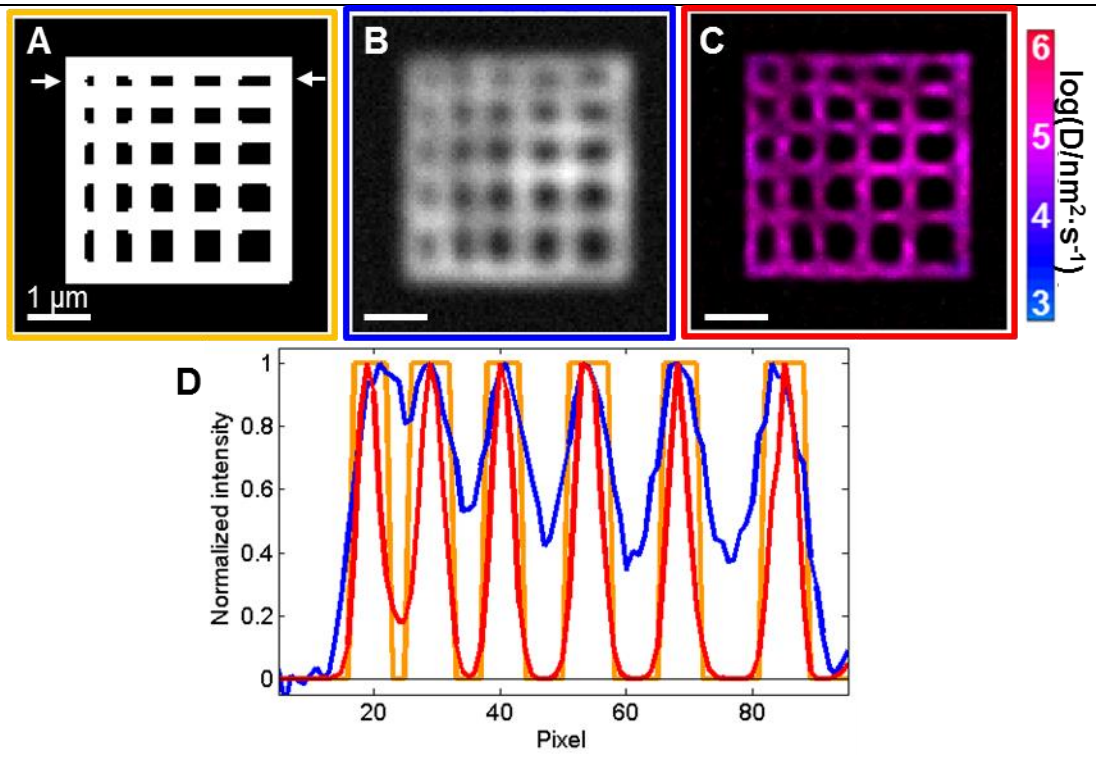

Figure S9. Two-dimensional simulation demonstrates super-resolution and diffusion coefficient capabilities of fcsSOFI analysis.
Two-dimensional Brownian diffusion of 25 emitters with D = 1 x 10^5 nm^2/s was simulated within (A) a pore map consisting of a waffle pattern where pore sizes varied from 3 x 3 to 10 x 10 pixels in size. The pore map is a binary image where emitters are allowed to be at a position where the image is white, but not allowed where the image is black. The (B, blue) average diffraction-limited image and (C, red) fcsSOFI image results are compared spatially to the (A, orange) "true" pore map in (D). (D) Reports the normalized intensity of a line section trace taken across the row of the smallest pores indicated by the arrows in (A). The average image does not resolve the separation of the two smallest pores at the leftmost side of the image (~ pixel 25). While the fcsSOFI image does resolve the separation for all the pores as judged at the fwhm, the pore width is less than the true value due to over-deconvolution effects. The diffusion properties were accurately calculated to be D_{calc} = 1.0 (± 0.4) x 10^5 nm^2/s by fcsSOFI. The intensity variation within the image is due to sampling (apparent concentration) effects that will be subject to future study understanding the relation between the experimental parameters, such as emitter concentration and number of frames collected, and the final resulting correlation images.[4]

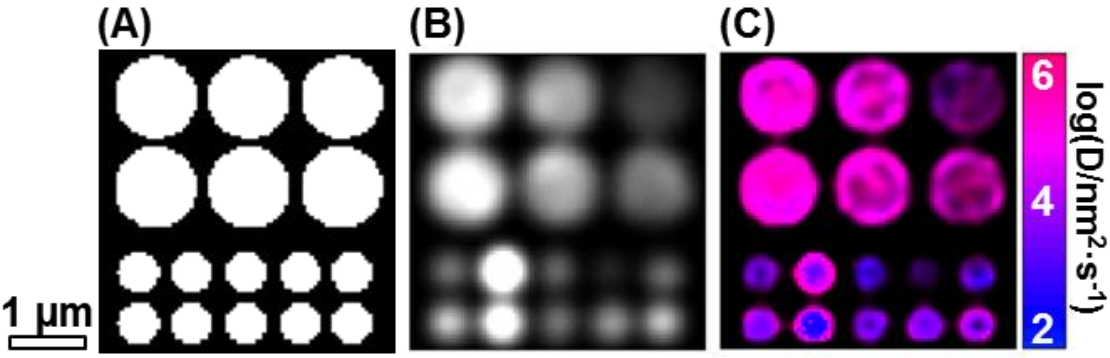

Figure S10. Two-dimensional simulation of varying pore sizes shows confinement effects the accuracy of calculating the diffusion coefficient.
Two-dimensional Brownian diffusion of 15 emitters with a $D = 1 \times 10^5$ nm^2/s was simulated within (A) the pore map consisting of large (diameter of 21 pixels) and small (diameter of 10 pixels) pores. (B) The average diffraction-limited image shown for comparison. (C) The fcsSOFI analysis result using Brownian diffusion models in Equations 7 and 8. First, the diffusion coefficients in the larger pores are correctly found to be $\log(D/\text{nm}^2 \cdot \text{s}^{-1}) = 4.9 \pm 0.2$. Emitters in the smaller pores incorrectly are underestimated to have a $\log(D/\text{nm}^2 \cdot \text{s}^{-1}) \sim 2 - 4$, despite all emitters having the same simulated diffusion coefficient. The confined environment in the small pores no longer allows the diffusion to be Brownian and an anomalous confined diffusion model should be used instead to accurately understand the transport. Application of a variety of models[6] to understand the diverse diffusion models will be subject of future work. Next, the resolution to resolve the adjacent boundaries of multiple pores is demonstrated by the improved contrast of the edges in (C) compared to (B). See earlier discussion of Equation S1. Finally, the intensity variation within the image is due to sampling (apparent concentration) effects as discussed in the caption of Figure S8. This is especially apparent in this simulation since emitters were randomly assigned to different pores and some of the confined pores had multiple emitters. All images measure 80 x 80 pixels, or 4 x 4 µm in size.

Supplementary studies on experimental data:

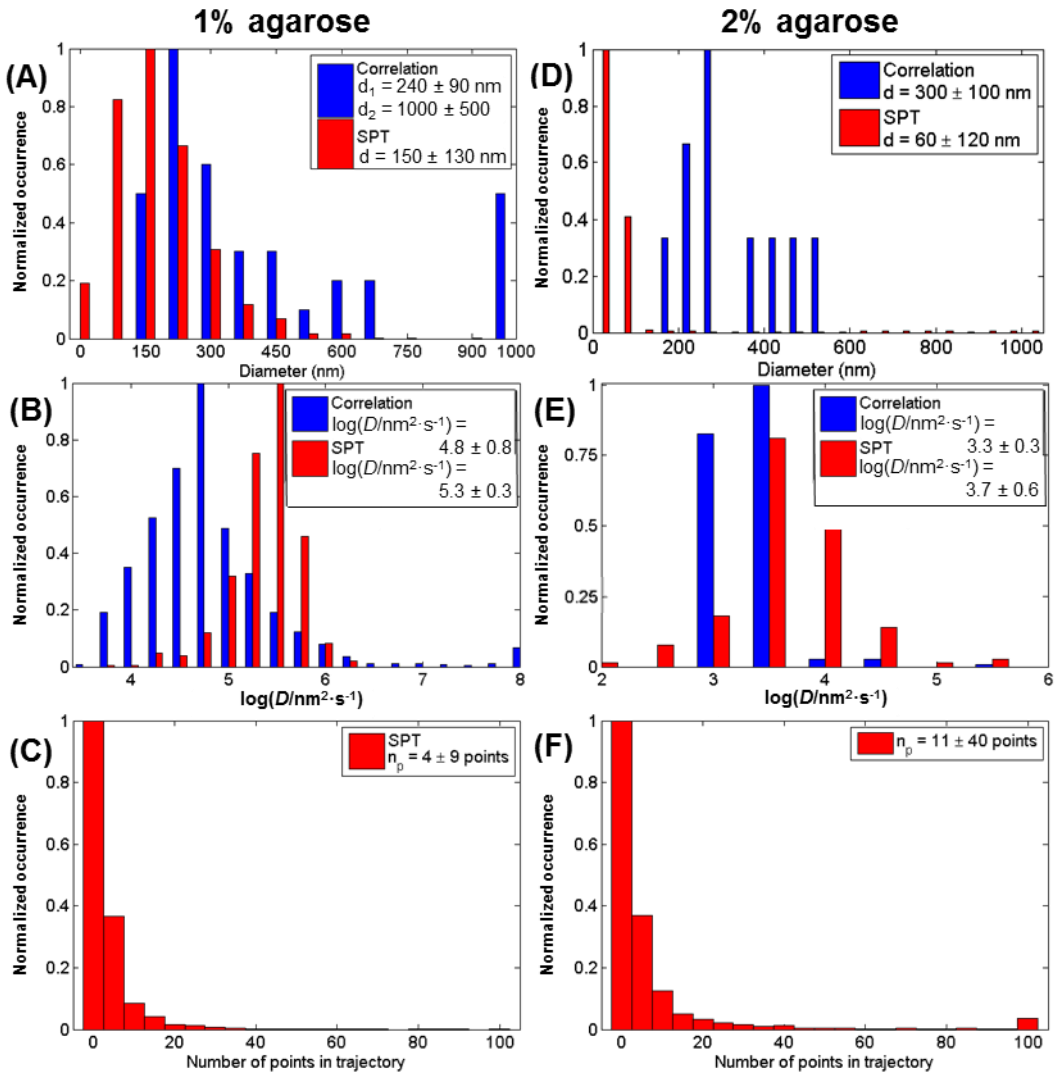

Figure S11. Quantitative histograms of 1% and 2% agarose statistics by fcsSOFI and single particle tracking analysis in Figure 2.
Results for (A-C) 1% agarose and (D-F) 2% agarose. (A, D) Pore diameter obtained by (blue) Delaunay triangulation analysis of the fcsSOFI image and (red) diameter of gyration analysis of the single particle tracking trajectories. The second population of pore size in the fcsSOFI analysis of 1% agarose (1000 ± 500 nm) was calculated by taking the average and standard deviation of the size of all pores that fall outside of three times the standard deviations of the normal distribution population of 240 ± 90 nm. (B, E) Distribution of log(*D*) obtained from (blue) curve fitting of fcsSOFI according to Equations 7 and 8 and (red) maximum likelihood estimation of analyzing the mean square displacements from single particle tracking.[5] (C, F) The length of the single particle tracking trajectories analyzed. The legends report the mean and standard deviations.

Further discussion of 2% agarose results.

The fused fcsSOFI image of immobilized emitters in 2% agarose has similar spatial and diffusion information to the diffraction-limited average images and single particle tracking. Similar analysis of the 100 nm emitters in 2% agarose (Figure 2c, f, i) was performed (Figure S9d, e, f). The 2% agarose has smaller pores that essentially immobilized the emitters. The correlation signal arises more from variation in the fluorescent intensity of the beads than diffusion. The diffusion coefficient was calculated to be $\log(D/\mathrm{nm}^2 \cdot \mathrm{s}^{-1}) = 3.3 \pm 0.3$ by fcsSOFI, the resolution of our instrument.[7] Single particle tracking had a similar result of $\log(D/\mathrm{nm}^2 \cdot \mathrm{s}^{-1}) = 3.7 \pm 0.6$, but had a larger average and spread due to some incorrect assignments of emitters moving between two pores when they were in close proximity (Figure 2i, green trajectory in bottom center), resulting in an overestimation of the diffusion coefficient. For the pore size, single particle tracking localized the centroids of the particles, reporting the resolution of the localization, 60 ± 120 nm. A result of 300 ± 100 nm was observed for fcsSOFI analysis, essentially reporting on the absolute size (~2σ) of the correlation-improved point spread function. Therefore, fcsSOFI analysis may not be the preferred method for analysis of stationary emitters that are trivial to track.

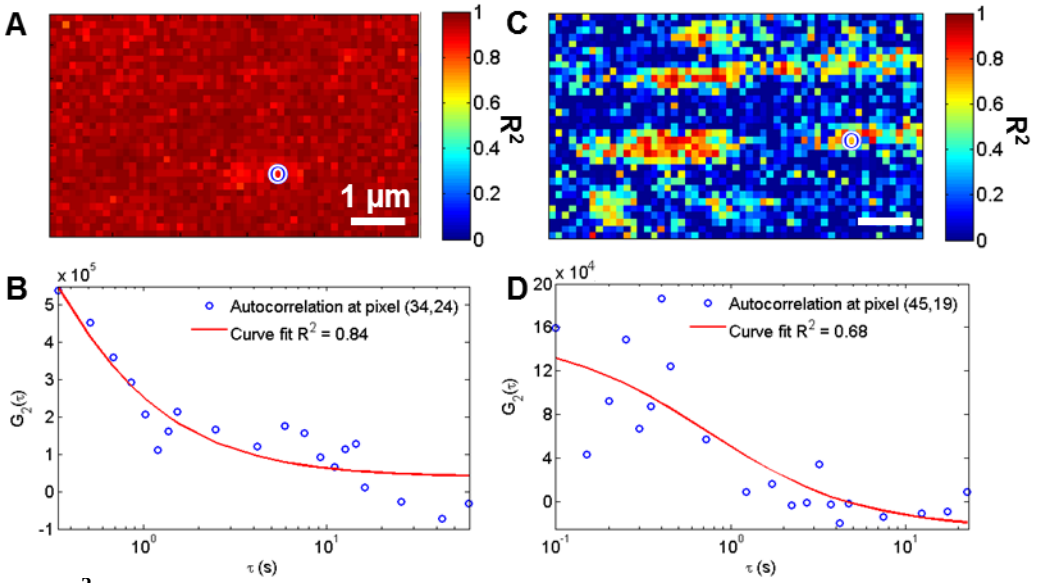

Figure S12. R^2 distribution and example curve-fitted autocorrelation data to obtain diffusion information of F127 and C12EO10 samples in Figure 3.
(A,B) Data from F127 and (C, D) C10EO12 in Figure 3. (A, C) Map of R^2 values obtained from curve fitting of autocorrelation curves. (B, D) Representative autocorrelation data and curve fit results for the pixels indicated by the blue circles in (A, B). In C12EO10 most of the R^2 values were very low ($R^2 < 0.7$) due to the challenging experimental conditions. Scale bars 1 µm.

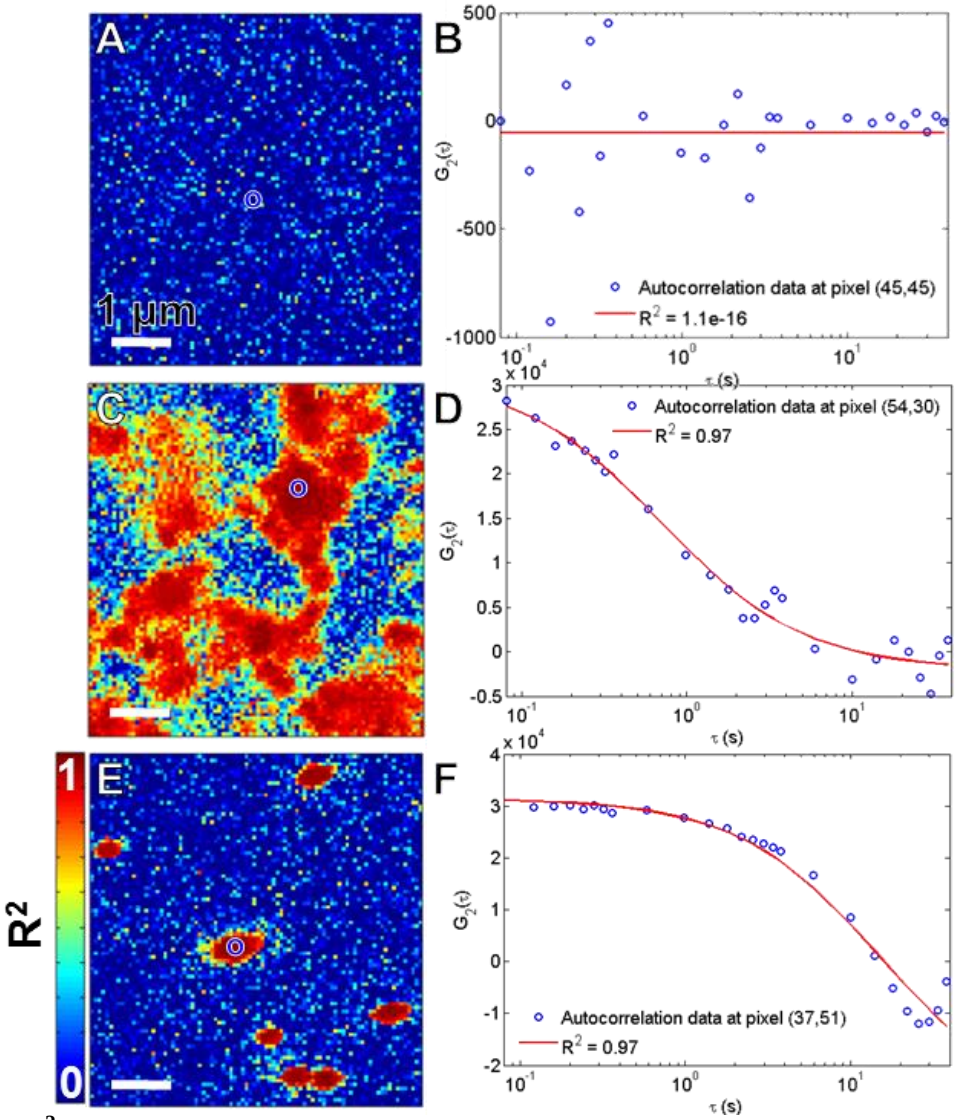

Figure S13. R^2 distribution and example curve-fitted autocorrelation data to obtain diffusion information of blank, 1% and 2% agarose samples in Figure 2.
(A, B) Data from blank, (C, D) 1% agarose, and (E, F) 2% agarose in Figure 2. (A, C, E) Map of R^2 values obtained from curve fitting of autocorrelation curves. (B, D, F) Representative autocorrelation data and curve fit results for the pixels indicated by the blue circles in (A, B, E). For the blank the R^2 values were very low since diffusion was very fast and no pores were present. Data reported in Figure 2d did not discard any of the R^2 data < 0.5 as all of the data would be discarded (see "Analysis: fcsSOFI" section in Methods). This data was the only exception to the R^2 cutoff. High confidence in the curve fitting (R^2 > 0.95), and hence, in the resulting diffusion coefficients, were observed for 1% and 2% agarose. Scale bars 1 µm.

Movies S1-8: Still frames and descriptions of Movies available as .avi for download.

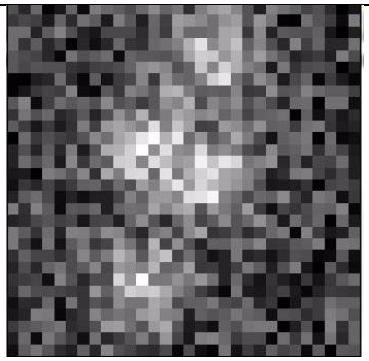

Movie S1. Simulation used in Figure 1. One-dimensional simulation at low signal-to-background ratio used in Figure 1 at signal-to-background ratio of 2. Image measures 1.5 µm x 1.5 µm, frame rate of 25 Hz.

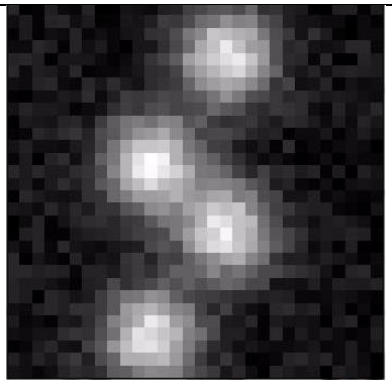

Movie S2. One-dimensional simulation at high signal-to-background ratio used in Figure S6. Image measures 1.5 µm x 1.5 µm, frame rate of 25 Hz, signal-to-background ratio of 10.

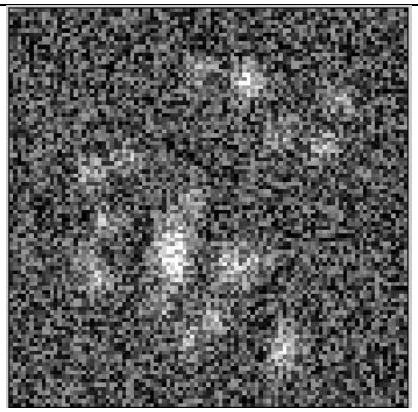

Movie S3. Two-dimensional simulation used in Figure S8. Image measures 5 µm x 5 µm, frame rate of 25 Hz, signal-to-background ratio of 1.

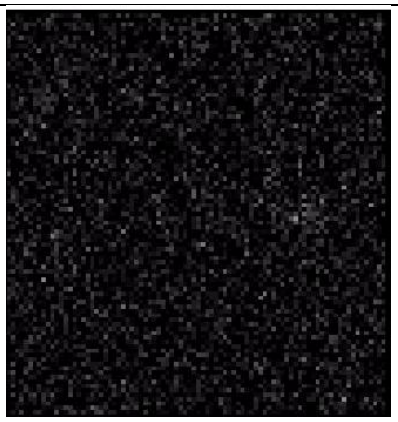

Movie S4. 100 nm beads in water over a blank coverslip used to produce Figure 2a, d, g. Image measures 5.7 µm x 5.7 µm, frame rate of 25 Hz.

Movie S5. 100 nm beads in 1% agarose used to produce Figure 2b, e, h. Image measures 5.7 µm x 5.7 µm, frame rate of 25 Hz.

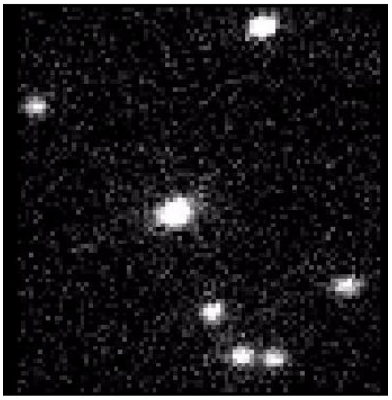

Movie S6. 100 nm beads in 2% agarose used to produce Figure 2c, f, i. Image measures 5.7 µm x 5.7 µm, frame rate of 25 Hz.

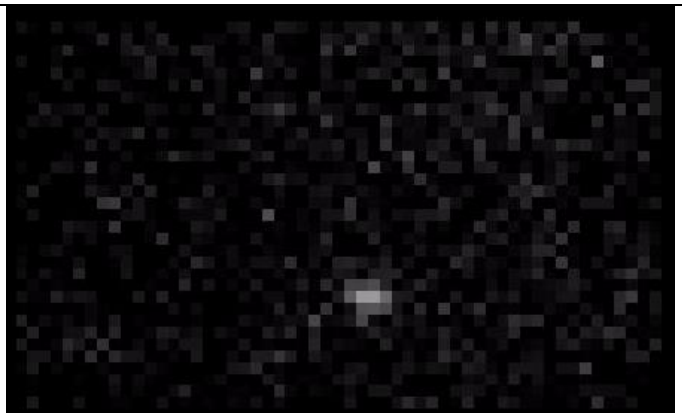

Movie S7. DTPDI in F127 used to produce Figure 3a, c, e. Image measures 6.8 µm x 4.1 µm, frame rate of 5.8 Hz.

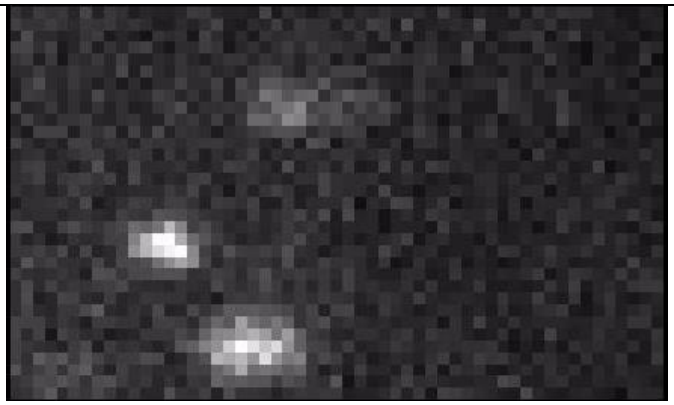

Movie S8. DTPDI in C12EO10 used to produce Figure 3b, d, f. Image measures 6.8 µm x 4.1 µm, frame rate of 20 Hz.

References

1. Schwille, P.; Haustein, E. Fluorescence Correlation Spectroscopy - an Introduction to Its Concepts and Applications. *Biophysical J. Online* **2002**.

2. Dertinger, T.; Pallaoro, A.; Braun, G.; Ly, S.; Laurence, T. A.; Weiss, S. Advances in Superresolution Optical Fluctuation Imaging (SOFI). *Q. Rev. Biophys.* **2013**, *46*, 210-221.

3. Lam, J. D.; Culbertson, M. J.; Skinner, N. P.; Barton, Z. J.; Burden, D. L. Information Content in Fluorescence Correlation Spectroscopy: Binary Mixtures and Detection Volume Distortion. *Anal. Chem.* **2011**, *83*, 5268-5274.

4. Tcherniak, A.; Reznik, C.; Link, S.; Landes, C. F. Fluorescence Correlation Spectroscopy: Criteria for Analysis in Complex Systems. *Anal. Chem.* **2008**, *81*, 746-754.

5. Shuang, B.; Byers, C. P.; Kisley, L.; Wang, L.-Y.; Zhao, J.; Morimura, H.; Link, S.; Landes, C. F. Improved Analysis for Determining Diffusion Coefficients from Short Single-Molecule Trajectories with Photoblinking. *Langmuir* **2013**, *29*, 228-234.

6. Kolin, D. L.; Wiseman, P. W. Advances in Image Correlation Spectroscopy: Measuring Number Densities, Aggregation States, and Dynamics of Fluorescently Labeled Macromolecules in Cells. *Cell Biochem. Biophys.* **2007**, *49*, 141-164.

7. Tauzin, L. J.; Shuang, B.; Kisley, L. M.; Mansur, A. P.; Chen, J.; de Leon, A.; Advincula, R. C.; Landes, C. F. Charge-Dependent Transport Switching of Single Molecular Ions in a Weak Polyelectrolyte Multilayer. *Langmuir* **2014**, *30*, 8391-8399.